

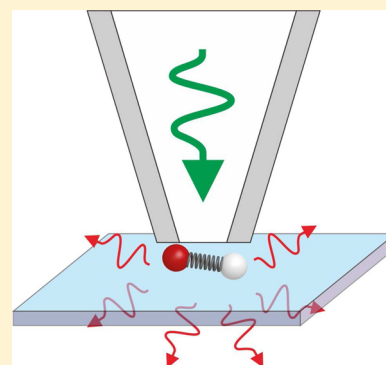
Near-Field Raman Spectroscopy with Aperture Tips

Weihua Zhang,[‡] Zheyu Fang,^{*,†} and Xing Zhu[†]

[†]School of Physics, State Key Lab for Mesoscopic Physics, and Collaborative Innovation Center of Quantum Matter, Peking University, Beijing 100871, China

[‡]College of Engineering and Applied Sciences, National Laboratory of Solid State Microstructures, and Collaborative Innovation Center of Advanced Microstructures, Nanjing University, Nanjing 210093, China

ABSTRACT: In this paper, we review nano-Raman techniques based on aperture scanning near-field optical microscopy (SNOM). Fundamentals of SNOM and aperture-tip-based near-field Raman spectroscopy and their applications in key technical issues, including Raman signal intensity and collection time, are introduced. Recent advances in the tip design are discussed, and applications of the aperture-SNOM-based nano-Raman technique are presented. We attempt to identify the most pressing open questions in this field. We believe that, by improving the power transmission efficiency and combining the local field enhancing technique with the tip-enhanced spectroscopy, the performance of aperture-SNOM can be significantly improved. Its nanometer-scale excitation volume and the consequent low background make the aperture-tip technique feasible for many important samples that cannot be measured by other optical nanospectroscopies.



CONTENTS

1. Introduction	5095
2. Scanning Near-Field Optical Microscope	5097
2.1. Optical Near-Fields for Super-Resolution Imaging	5097
2.2. Tip–Sample Distance Control	5097
2.3. Conventional Aperture Tips	5097
2.3.1. Tapered Fiber Tips	5097
2.3.2. Optical Transmission Coefficient of Tapered Fiber Tips	5098
2.3.3. Other Aperture Tips	5098
3. Near-Field Raman Nanospectroscopy	5098
3.1. Raman Spectroscopy	5098
3.2. General Setup	5099
3.3. The Signal Strength in Near-Field Raman Spectroscopy	5099
3.3.1. Signal Strength in Micro-Raman	5099
3.3.2. Signal Strength of Near-Field Raman Excited by an Aperture Tip	5100
3.3.3. Signal Strength in Tip-Enhanced Raman Spectroscopy	5100
4. Application of Near-Field Raman Spectroscopy	5100
4.1. Nonresonant Near-Field Raman Detection of Inorganic Materials	5101
4.2. Near-Field Resonant Raman Scattering	5102
4.3. Near-Field Study of SERS Using Aperture Tips	5103
4.4. Near-Field Raman Spectroscopy at Liquid–Liquid Interfaces	5104
5. Recent Advances in Tip Design	5105
5.1. Extraordinary Transmission	5105
5.2. Nanostructured Aperture Tips	5105

5.3. Plasmonic-Waveguide-Based Near-Field Tip	5105
6. Perspective	5106
Author Information	5106
Corresponding Author	5106
ORCID	5106
Notes	5106
Biographies	5106
Acknowledgments	5107
References	5107

1. INTRODUCTION

New technologies and tools often play the role of the engine in the progress of modern science. Optical microscopy is one great example that pushed the boundary of the visual world of human being from the submillimeter to micrometer scale and changed our understanding of nature profoundly. For instance, the invention of Leeuwenhoek's single-lens microscope, which "far surpass those which we have hitherto seen",¹ directly led to the birth of a new field, microbiology. In addition to high spatial resolution, optical microscopy is also capable of revealing spectral information, allowing one to identify the material of a tiny sample via its "color" in ambient environment without sample preparation. Thanks to these unique capabilities, the optical microscope has become an indispensable tool for fast, nondestructive, microscale chemical analysis.

Among the variety of microspectroscopic analytical methods, Raman spectroscopy is one of the most powerful techniques. As

Special Issue: Vibrational Nanoscopy

Received: May 30, 2016

Published: December 15, 2016

a vibrational spectroscopy, Raman spectra provide the frequency of a substance's vibrational modes, which reflect information on the chemical and physical forms and can be used to identify substrates from their "fingerprint" spectral patterns.^{2–4} Moreover, Raman measurements are simple, rapid, and extremely flexible. One can directly measure a given sample without preparation, no matter whether it is liquid or solid, organic or inorganic, crystalline or amorphous. Because of these advantages, micro-Raman techniques have been emerging as one of the most important mapping tools for chem-/bioanalysis, especially after the major innovations in the 1970s and 1980s, namely, the charge-coupled device (CCD), compact spectrograph, effective laser rejection filter, near-infrared laser, and small computer.^{5,6}

After the 1990s, driven by the demands of fast-growing nanoscience and nanotechnology, researchers started to develop new techniques in order to push the spatial resolution of Raman spectroscopy into the nanometer scale. However, in this process, a fundamental obstacle, the diffraction limit, was encountered. It states that one cannot distinguish two points within the region around half of the wavelength of the incident light.⁷ The diffraction limit is also known as Abbe's criteria, named after the German physicist Ernst Abbe, who derived the diffraction limit in theory in 1873.⁸ Abbe realized that the high spatial frequency components of light cannot reach the far-field zone (consequently, detectors) due to the wave nature of light, and it is a fundamental limit for the resolution of the optical microscopy. Interestingly, this theory also hints that there is an unknown world awaiting exploration, named the evanescent field, which is bound in the optical near-field regime of sample surfaces (i.e., within one wavelength), containing detailed information on samples.

After Abbe reported his theory, within almost half a century, people tried many different ways to circumvent the diffraction limit, until E. H. Syngé realized the importance of the evanescence waves and introduced the concept of the optical near-field in his paper "Method for Extending the Microscopic Resolution into the Ultra-Microscopic Region" in 1928.⁹ In that paper, Syngé suggested that one can break the diffraction limit by bringing a subwavelength aperture into the near-field regime and pick up the high-spatial frequency information on the sample for the far-field detector. Syngé's proposal requires a stable control of the sample–aperture distance with sub-wavelength precision, typically in the 10 nm range, which was prohibitively difficult in the optical regime in his age. Indeed, due to the technical difficulty of microfabrication, the first experimental demonstration of a near-field microscope was performed in the microwave regime by Ash and Nicholls in 1972.¹⁰ In their work, the spatial resolution of $\lambda/60$ was achieved. The use of a subwavelength aperture in the visible spectral regime was not possible until the development of the scanning tunneling microscope (STM),¹¹ which provided the technical approach by which a metallic probe could be held only nanometers away from the sample surface. The first scanning near-field optical microscope (SNOM or NSOM) was demonstrated in 1984 by the two independent laboratories of Pohl and Lewis with an optical resolution on the order of $\lambda/10$.^{12,13}

One of the milestones of the SNOM technique is the detection of single-molecule fluorescence in real-space at the room temperature. In the early 1990s, Betzig et al. reported the first single-molecule fluorescence image by using an improved tapered fiber tip¹⁴ that was coated by a metallic layer to create a

nanoaperture.¹⁵ This aperture-SNOM then became a standard tool for nanospectroscopic analysis ever since, with which a large variety samples were measured with a spatial resolution down to 50 nm.¹⁶

Encouraged by the success in fluorescence detection, in order to reach the goal of nanoscale chemical analysis, many attempts have also been made to combine the SNOM with spectroscopic techniques, including mass spectrometry,^{17,18} infrared spectroscopy¹⁹ and, particularly, Raman spectroscopy.²⁰ For instance, In 1995, Smith and co-workers performed the first molecule near-field Raman experiment with a subwavelength aperture probe held in the near-field by using a shear-force feedback mechanism.²¹ Anger et al. collected near-field Raman spectroscopy of Rhodamine 6G (R6G) dye molecules at cryogenic temperatures.¹⁶

Despite a few successful experimental demonstrations, the aperture-tip-based near-field Raman spectroscopy (AT-NFRS) did not show itself to be a key nanoscale analytical tool. One of the major obstacles is that the near-field Raman signals were extremely weak, since the normal Raman scattering cross-section is approximately 10^{-30} cm²/sr, more than 10 orders of magnitude smaller than the absorption cross-section of fluorescent dye molecules.^{3,22} As a result, a longer collection time is required to obtain a reasonable signal-to-noise ratio. Another important reason is that, in practice, the spatial resolution of aperture SNOM was limited to 50 nm due to the extremely low transmission coefficient of aperture tips. It was demonstrated in both experiment and theory that, when the aperture diameter is shrunk below 50 nm, the power transmission coefficient of a fiber-based aperture tip drops below 10^{-4} ,²³ which is too weak to be detected in practice.

To improve the spatial resolution, researchers developed another approach, called apertureless SNOM, which utilizes a sharp metal tip to scatter the light field from the optical near-field to the far-field. Because it does not require an aperture to deliver light, the spatial resolution is only limited by the radius of the tip curvature, which can reach below 10 nm routinely today. Depending on the near-field signal retrieval method, there are two major types of apertureless-SNOM, namely, scattering SNOM, which detects the Rayleigh scattering signal,^{19,24} and tip-enhanced Raman spectroscopy (TERS), which uses the near-field enhancement on sharp metal tips to detect Raman scattering signals in the vicinity of the tip apex.^{25–27} It is worth noting that today the scattering-SNOM-based nanoscale IR spectroscopy technique is an important nanoscale analysis tool in parallel to the near-field Raman techniques²⁸ and has been nicely reported by other review papers.^{29,30} Here, we limit our discussion to the field of near-field Raman analysis techniques.

In the past decade, TERS enjoyed a huge success. With a "hot" tip, researchers were able to see the Raman signal from a single molecule,^{31–33} even from a single chemical bond with spatial resolution down to 1 nm.^{34,35} However, there are costs for the high sensitivity and resolution. Because there is no nanoaperture to deliver the excitation light, far-field excitation is needed and consequently brings a high background intensity.^{36–38} In addition, the high enhancement makes contamination fatal to TERS tips, since any adsorbate on the tip apex can give a significant rise to the background. On the other hand, the aperture SNOM technique is naturally immune to these issues. Particularly, recent results show that the performance of nanoapertures can be significantly improved with new designs, and the aperture SNOM technique started to

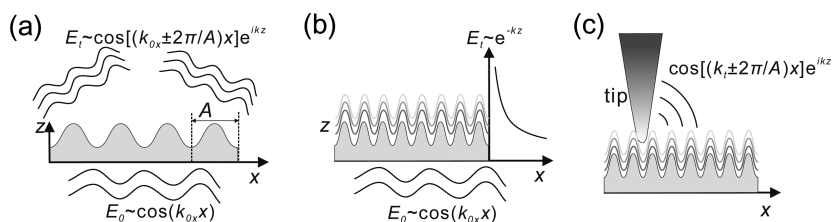


Figure 1. Spatial frequency mixing on grating samples. (a) Low-spatial-frequency information can propagate into the far field. (b) High-spatial-frequency information is carried by evanescent waves, which are bounded on the grating surface. (c) Evanescent waves can be converted into detectable waves by a sharp tip.

regain researchers' interests.³⁹ Herein, we present a critical review on AT-NFRS with an emphasis on technical issues and possible solutions, as well as the future perspective.

This review is organized as follows. First, the fundamentals of SNOM are introduced. Then, the AT-NFRS technique with emphasis on key technical issues is reviewed, including Raman signal intensity, collection time, and applications. After that, the recent advances in the design of aperture tips are discussed, and the future perspective is presented.

2. SCANNING NEAR-FIELD OPTICAL MICROSCOPE

2.1. Optical Near-Fields for Super-Resolution Imaging

The central idea of SNOM is to use a subwavelength tip to convert high-spatial-frequency components from the optical near-field into detectable far-field propagating waves. To illustrate this process, we take a grating sample as an example, as shown in Figure 1. When grating with a spatial frequency of $k_s = 2\pi/A$ (A is the period) is illuminated, the excitation field $E_0 \sim \cos(k_{0x}x)$ is modulated by the sample, and the mixing of spatial frequency occurs. The spatial frequency k_x of the transmitted light in the x -direction becomes $k_{0x} \pm k_s$, where k_{0x} is the x component of the wave vector of E_0 . In the free space, $k_{0x} < 2\pi/\lambda$ and $k_x^2 + k_z^2 = (2\pi/\lambda)^2$. Therefore, if $|k_{0x} \pm k_s| > 2\pi/\lambda$ (i.e., $k_s > 4\pi/\lambda$), k_z becomes imaginary, and evanescent waves can be generated. In other words, all the detailed sample information with high spatial frequencies are bounded in the optical near-field on the sample surface and cannot be observed in the far-field, which leads to the light diffraction limit.⁴⁰

In a SNOM setup, nanometer-sized tips carrying large spatial frequencies ($|k_t| > 2\pi/\lambda$) are used. This allows the conversion of high-spatial-frequency components of the sample into detectable low-frequency components via frequency mixing (i.e., $|k_t \pm k_s| < 2\pi/\lambda$) and the breaking of the diffraction limit. Although the physics is clear, practically, it is challenging to realize such near-field frequency mixing, because it needs nanometer-sized optical tips and the high-precision control of the tip-sample distance. To date, a large number of techniques have been developed to overcome those challenges, and in the following, a brief retrospect of the key developments is presented.

2.2. Tip-Sample Distance Control

Practically, a stable control of the tip-sample distance within 10 nm is commonly needed to achieve an efficient near-field excitation. In fact, this stringent requirement was one of the major reasons why SNOM was not realized until the invention of STM.^{11,13} Indeed, at the early stage, electronic tunneling of the STM technique was the main method for tip-sample distance control in SNOM. However, because the tunneling current technique needs conductive samples, it was gradually replaced by other techniques later.

Today, the shear-force approach is the most used method for tip-sample distance control in SNOM.^{11,13} In the shear-force method, the tip vibrates in the direction parallel to the sample surface at its resonance frequency. When the tip-sample distance is smaller than 20 nm, shear-forces arise at the resonance frequency, and consequently, the amplitude and phase of the vibration are modulated. To detect such a weak vibration, optical detection methods, particularly interference-based techniques, were first introduced.^{41–43} However, due to the undesired optical background induced by the optical detection, later it was replaced by a nonoptical technique, the tuning fork technique that was introduced by Karrai and Grober.⁴⁴ In their configuration, a tuning fork is mounted alongside the tip and made to oscillate at its resonance frequency. The amplitude is closely related to the tip-sample distance. It is therefore possible to control the tip-sample distance by using the vibrational signal of the tip in a way similar to the case of the noncontact atomic force microscope (AFM). In practice, the vibration amplitude of the tip in the shear-force mode is smaller than 5 nm (today, it is normally smaller than 1 nm).

It is worth noting that the tuning-fork-based tip-sample distance control technique is one of the key innovations in SNOM. It is sensitive and can detect sub-piconewton forces in the ambient area,⁴⁴ allowing a stable control of fragile fiber tips. Although originally it was used to detect the shear force, the tuning fork method was soon extended to the tapping mode, where the tip is vibrating perpendicular to the sample surface.⁴⁵ Particularly, in a vacuum, the tuning fork shows an extremely high sensitivity. With the help of the Q-plus technique and phase-lock-loop technique, today people can even resolve the topology of single atoms in an ultra-high-vacuum environment.^{46–48}

2.3. Conventional Aperture Tips

2.3.1. Tapered Fiber Tips. Making high-performance optical tips is a requirement of SNOM. By far, the aperture probe made of metal-coated tapered fibers is the most widely used SNOM tip, because fiber tips are cheap and simple to fabricate and can be conveniently coupled to laser sources and detectors thanks to the rich fiber-optic tools in the market.

There are two major ways to fabricate the tapered fiber tip, i.e., pulling and etching. The pulling technique was originally used for the fabrication of a patch clamp, in which quartz micropipettes were heated by a CO₂ laser and pulled subsequently to form a hollow probe. Later, this method was adapted to make tapered fiber tips with all of the parameters investigated in great detail.⁴⁹ Fiber tips made by this pulling technique have a smooth surface (Figure 2a). However, their power transmission efficiency is low because the taper angle of the pulled fiber is small (commonly smaller than 10°). The etching technique, on the other hand, can produce tips with a

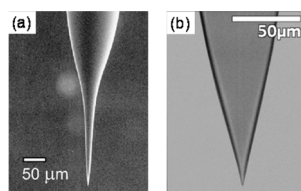


Figure 2. Tapered fiber tips fabricated by thermal pulling (a) and chemical etching (b). Reproduced with permission from ref 56. Copyright 2000 AIP Publishing LLC.

large taper angle, but the surface smoothness and reproducibility are poor.⁵⁰ To solve these issues, a variety of etching techniques were developed, for example, the tube etching technique developed by Zenobi and co-workers, which utilized the circulating flow of HF acid that formed in the plastic protection tube of the fiber to create a smooth tip surface.^{51–53} Another important method was developed by Ohtsu and co-workers, who successfully obtained a sharp and short protrusion with a varied apex angle by utilizing the low etching rate of a Ge-rich fiber (Figure 2b).^{54,55}

2.3.2. Optical Transmission Coefficient of Tapered Fiber Tips. The transmission coefficient and aperture size are the most important optical parameters of an aperture tip, and many theoretical works have been reported on the relation between them. The most widely used model is the Bethe–Bouwkamp theory, which describes the far-field and near-field properties of light transmitted through a circular subwavelength aperture.^{57,58} It shows that the far-field radiation of a subwavelength aperture is equivalent to the far-field radiation of a radiating magnetic dipole, consistent with the Babinet’s principle.⁵⁹ Despite the broad usage, the Bethe–Bouwkamp theory is an oversimplified theory. It assumes a deep subwavelength aperture on a flat screen made of a perfect conductor, which is different from real experiments. To address this issue, other techniques were also developed. For example, Novotny and Hafner analyzed the power transmission by treating the tip as a lossy waveguide.²³ Their results indicate that the power transmission is sensitive to the aperture size and taper angle. For a 20 nm aperture on a narrow (10 degree) tapered tip, only 10^{-12} of the incident power can go through the aperture, and most of the incoming light is reflected or becomes heat due to the absorption of the metal coating. Another important factor influencing the power transmission efficiency is the taper angle, δ . The mode-matching theory shows that the transmission can be described by a simple relation:

$$\frac{P_{\text{out}}}{P_{\text{in}}} \propto e^{-B \cot \delta} \quad (1)$$

Here B equals 3.1 for a 20 nm aperture excited at 488 nm.⁷ The result shows that the power transmission can be improved by 9 orders of magnitude by changing the taper angle from 10° to 45° . Methods for fabricating sharp fiber tips with a large taper angle are therefore crucial for aperture SNOM.

In addition to the power transmission efficiency, the brightness of the aperture tip is also related with the damage threshold, which decides how much power one can couple into the tip without causing damage. It is possible to improve the brightness of an aperture probe by optimizing its metal coating.^{51,60} More recently, in the field of plasmonics, it was found that the thermal stability of a metallic structure can be improved substantially by depositing a thin layer of Al_2O_3 on it

by atomic layer deposition (ALD). With the advance of thin-film techniques, one can expect significant increase of the damage threshold for aperture tips in the future.

2.3.3. Other Aperture Tips. Besides the fiber tip, in order to achieve a large taper angle, other types of aperture probes were also developed. One example is the metal-coated pyramid probe fabricated by Minh et al.⁶¹ The tip was made of a SiO_2 pyramid on a Si cantilever and can be directly used in a commercial AFM instrument (Figure 3b). With a large apex

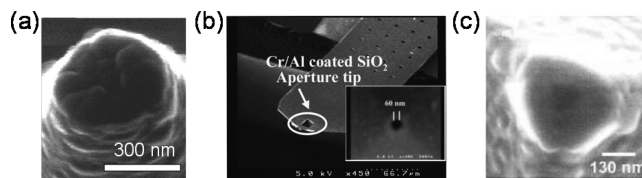


Figure 3. Aperture probes. (a) Al-coated tapered fiber tip. Reproduced with permission from ref 56. Copyright 2000 AIP Publishing LLC. (b) Metal-coated SiO_2 pyramid tip on a Si cantilever. Reproduced with permission from ref 61. Copyright 2000 AIP Publishing LLC. (c) Al-coated tetrahedral probe with a 30 nm aperture. Reproduced with permission from ref 62. Copyright 2002 American Physical Society.

angle, this type of tip exhibits a high power transmission, and in the original paper, 1% power transmission was reported with a 100-nm-sized aperture. Another interesting type of aperture tip is the aperture-tetrahedral tip developed by Fischer (Figure 3c). With a relatively high power transmission, a spatial resolution of 30 nm was demonstrated.⁶²

3. NEAR-FIELD RAMAN NANOSPECTROSCOPY

Soon after the invention of SNOM, researchers started to realize the potential of SNOM in nanoscale chemical analysis by using Raman spectroscopy. Countless efforts were made to develop the near-field Raman technique. In this part, we present a retrospect of aperture-SNOM-based Raman spectroscopy and discuss its key parameters, such as spatial resolution and signal-to-noise ratio, in comparison with other Raman imaging techniques.

3.1. Raman Spectroscopy

Raman spectroscopy is a type of vibrational spectroscopy, named after the Indian physicist Chandrasekhara Venkata Raman, who discovered this phenomenon in the 1920s and received the Nobel Prize in 1930.^{63–65} Figure 4 shows basic processes that occur for a molecule to scatter light. The Raman frequency shifts reflect the strength of chemical bonds and can

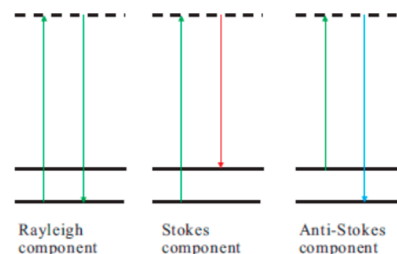


Figure 4. Energy diagram for Rayleigh and Raman scattering. Depending on the relative energy levels of the initial and final states, light scatterings can be classified into three groups, i.e., the Rayleigh scattering component, Stokes component, and anti-Stokes component.

be used as the “fingerprint” of the molecule. One can therefore identify chemical substances in a sample with Raman spectra.

The differential cross section of the normal Raman scattering (NRS) of a chemical bond, σ_{NRS} , is typically $10^{-31} \leq \sigma_{\text{NRS}} \leq 10^{-29} \text{ cm}^2/\text{sr}$ in the visible and near-infrared spectral regime.²² When the excitation wavelength is closed to the electronic transition wavelength, resonance Raman scattering (RRS) occurs and the cross-section, σ_{RRS} , can be as high as $10^{-24} - 10^{-23} \text{ cm}^2/\text{sr}$, several orders of magnitude larger than σ_{NRS} , but it is still 10 orders of magnitude smaller than the absorption cross-section associated with the electronic transition of a fluorescent molecule. Because of the extremely small scattering cross-section, Raman spectroscopy was not immediately implemented in real applications after its discovery. This situation did not change until the 1980s when the solid-state laser, notch filter, and high-quality charge-coupled device (CCD) were available.

3.2. General Setup

A typical near-field Raman microscope consists of a micro-Raman spectrograph and a near-field scanning unit with the tip aligned along the optical axis, as depicted in Figure 5. The near-

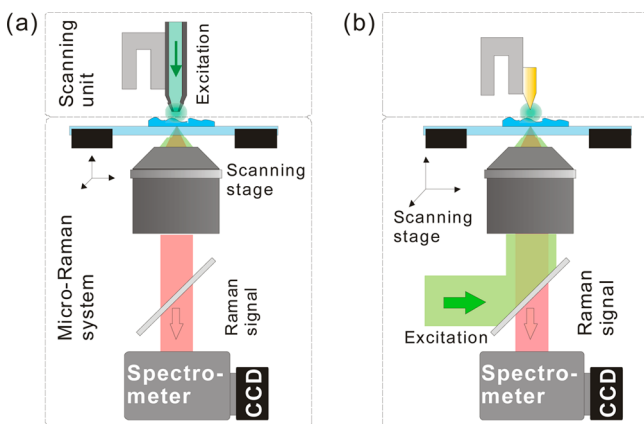


Figure 5. Schematic of near-field Raman microscope based on (a) aperture-SNOM and (b) apertureless-SNOM, (i.e., TERS).

field scanning unit functions as an additional zooming device, which extends the spatial resolution of the micro-Raman system into the nanometer scale. A typical scanning unit includes a coarse approaching motor in the z -direction and a feedback system that provides a stable control of the tip-sample distance.

Depending on the incident excitation, a near-field Raman microscope can be divided into two groups, an aperture-SNOM Raman spectrograph, which implements a tip with a nano-aperture to deliver laser excitation into the nanoscale, and a scattering-SNOM Raman spectrograph, which uses an apertureless tip with far-field excitation. In addition, there are also tips that do not have a physical aperture but utilize a tapered surface plasmon waveguide to confine the light into the nanoscale on the sample. In this work, we categorize this type of tip as an aperture tip, because their working principle, as well as the experimental setup, is similar to the conventional aperture-SNOM.

Commonly, a near-field Raman system is capable of performing both normal micro-Raman and near-field Raman spectral mapping. When the SNOM tip is retreated from the sample surface, the near-field Raman spectrograph can function

as a normal micro-Raman system. To do near-field Raman mapping, one only needs to bring the tip into the near-field regime and use it to excite the sample. To obtain an image, raster scanning is utilized in the near-field Raman system. Different from the commercial micro-Raman system, in which the beam-scanning mode is often implemented, most of near-field Raman systems choose the sample scanning, with which the tip (i.e., the excitation spot) can stay aligned with the collection optics throughout the mapping process.

3.3. The Signal Strength in Near-Field Raman Spectroscopy

One of the major challenges in the field of Raman spectroscopy, especially for the near-field Raman mapping, is that the Raman scattering cross section of molecules is extremely small. In the following, we discuss the Raman signal strength in the case of aperture SNOM and further make a comparison with the normal micro-Raman and TERS in order to show the limit and potential of the AT-NFRS technique.

3.3.1. Signal Strength in Micro-Raman. For simplicity, we start with the normal micro-Raman (i.e., the far-field Raman). The strength of the Raman signal depends on the sampling volume, V_{exc} , which is determined by the spatial resolution in both lateral and axial directions of the system, as

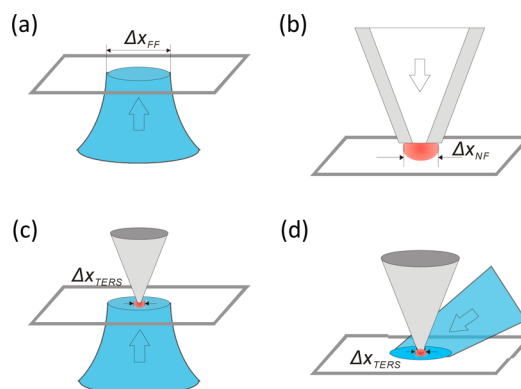


Figure 6. Schematic of different excitation methods for the Raman microscope: (a) conventional far-field micro-Raman, (b) AT-NFRS technique using a tapered fiber tip, and (c and d) TERS with transmission illumination and side illumination, respectively.

shown in Figure 6. For a micro-Raman system, the spatial resolution in the lateral and axial directions is

$$\Delta x_{\text{FF}} = 0.61 \frac{\lambda}{\text{NA}} \quad (2)$$

and

$$\Delta z_{\text{FF}} = \frac{2\lambda}{\text{NA}^2} \quad (3)$$

, respectively.⁷ Here, NA is the numerical aperture of the objective and λ is the excitation wavelength. If the density of the sample molecule (or bond) is n_{anal} , there are $N = n_{\text{anal}} V_{\text{exc}}$ molecules (or bonds) detected by the system, and the total Raman cross section of those molecule becomes $\Sigma = N\sigma$. Here, the coupling between molecules in the scattering process is neglected because the Raman scattering cross section of molecules (σ) is extremely small. Then the power of the Raman scattering is Σ/I_{exc} and can be written as

$$P_{\text{RS}} = \sigma_{\text{RS}} n_{\text{anal}} V_{\text{FF_exc}} I_{\text{exc}} \eta \quad (4)$$

Table 1. Raman Signal Strengths of Different Raman Techniques

	V_{exc} (nm ³)	A_{exc} (nm ²)	g_{exc} ⁴	P_{exc}	P_{RS} (W)
micro-Raman (NA = 0.9, 532 nm)	5×10^8	2×10^5	1	1 μ W–10 mW	10^{-14}
aperture SNOM (100 nm aperture)	10^6	$\sim 10^4$	10–100	1 nW–1 μ W	10^{-17} – 10^{-16}
TERS (10 nm tip)	10^3	10^2	10^3 – 10^7	~ 1 mW	10^{-14} – 10^{-10}

In practice, it is the excitation power, $P_{\text{exc}} = I_{\text{exc}} A_{\text{exc}}$ instead of the light intensity that is commonly used; we then write the power of the Raman signal as

$$P_{\text{RS}} = \frac{\sigma_{\text{RS}} n_{\text{anal}} V_{\text{FF_exc}}}{A_{\text{FF_exc}}} P_{\text{exc}} \eta \quad (5)$$

Here, η is the collection efficiency of the system and $A_{\text{FF_exc}} = \pi \Delta x^2 / 4$ is the cross-section of the far-field excitation in the lateral direction.

We take a pure organic molecule sample as an example. The typical differential cross-section is $\sim 10^{-30}$ cm²/sr for an organic molecule, and the total cross-section can reach 10^{-29} cm²/sr when an objective with a large NA is used. When it is excited by a 10 mW green laser (532 nm) via an objective with NA = 0.9, the excitation/sampling volume is around 1 fL. Assuming that there is ~ 1 molecule per 1 nm³, approximately 10^{10} molecules are excited. If the cross section of normal Raman scattering is 10^{-30} cm²/sr, there are about 10^4 photons ($\sim 10^{-14}$ W) exchanging energy with the photon modes and exhibiting a Raman shift. This is a very weak signal and can only be effectively measured by single-photon counting devices or advanced CCD cameras. This is the reason why micro-Raman was not broadly used for chemical analysis until the 1980s, when high-performance CCD cameras became available.

3.3.2. Signal Strength of Near-Field Raman Excited by an Aperture Tip. The signal strength in AT-NFRS measurements can be estimated using a similar approach. The major difference is that, instead of using a focused laser beam, the AT-NFRS implements a nanometer aperture to create a local light source. When the aperture size of the tip is much smaller than the wavelength of the light source, the light emitting from the tip can consist of wave vector components large than the wave vector of the light source because of the small aperture size. Different from the propagating components, there are strong near-field components, which cannot propagate into the far-field zone. The near-field components can be effectively described as the local field enhancement, as depicted in Figure 6b. Therefore, to calculate the Raman signal, an additional enhancement factor, $g_{\text{exc}} = |E_{\text{loc}}|^2 / |E_{\text{exc}}|^2$, needs to be added into eq 3. Moreover, due to the reciprocity in electromagnetism, the radiation process of the Raman scattering is also enhanced by a factor of $g_{\text{exc}} = |E_{\text{loc}}|^2 / |E_{\text{exc}}|^2$.²² Therefore, in the case of near-field Raman scattering, eq 4 becomes

$$P_{\text{RS}} = \sigma_{\text{RS}} n_{\text{anal}} V_{\text{exc}} I_{\text{exc}} g_{\text{exc}}^2 \eta \quad (6)$$

eq 6 can also be rewritten by substituting I_{exc} with $P_{\text{exc}} / A_{\text{NF_exc}}$

$$P_{\text{RS}} = \sigma_{\text{RS}} n_{\text{anal}} V_{\text{NF_exc}} \frac{P_{\text{exc}}}{A_{\text{NF_exc}}} g_{\text{exc}}^2 \eta \quad (7)$$

Here, $V_{\text{NF_exc}}$ and $A_{\text{NF_exc}}$ are the near-field excitation volume and area with an aperture probe.

In a typical aperture-SNOM, the size of the aperture (i.e., Δx_{NF}) is approximately 100 nm and the wave vector k_z along z -direction is about $\sqrt{(2\pi/\lambda_0)^2 - (2\pi/\Delta x_{\text{NF}})^2}$; thus, the

enhanced evanescent field is confined in a few tens of nanometers ($1/|k_z|$) in the z -direction, and the resulted excitation volume is approximately 10^5 nm³, which is 3 orders of magnitude smaller than the case of micro-Raman. Although the excitation area is 2 orders of magnitude smaller and there is often an enhancement factor of $|g_{\text{exc}}|^2$ normally in the range of 10–100-fold due to the nanoscale roughness on the tip, the resulting signal is roughly 2–3 orders of magnitude smaller than the case of micro-Raman. This low signal level makes AT-NFRS experiments extremely challenging and only doable for samples with strong Raman effects, such as pure samples, molecules with resonance-Raman effects, and surface-enhanced Raman substrates. In fact, even for a pure sample, such as diamond thin film, at least 1 min is needed to collect a Raman spectrum at one sampling point.⁶⁶

3.3.3. Signal Strength in Tip-Enhanced Raman Spectroscopy. In contrast to the aperture SNOM, TERS exhibits a much higher signal strength and even allows the detection of a single molecule, although the near-field excitation volume is 2–3 orders of magnitude smaller. The key to the high sensitivity in TERS is the giant local field enhancement generated at the sharp metal apex. When a metallic substrate is used, the enhancement factor can reach 10^7 or even larger, which leads to a signal $\sim 10^4$ times higher than normal micro-Raman measurements.^{37,38,67–70}

However, when a transparent bulk sample is used, the enhancement factor is often much smaller, normally in the range of 10^2 – 10^5 .⁷¹ In this case, the near-field Raman signal from the tip apex is comparable or even smaller than the background generated by the far-field excitation (Figure 6c,d), making it impossible to retrieve the near-field information. Especially, in the case of thick samples, one needs to use a long working distance objective lens (consequently, a small NA) to excite and collect light from the side (Figure 6d), and this leads to an even higher background (such as fluorescence of the substrate and noise) than in the case of transmission type TERS (Figure 6c).

Today, the high background induced by far-field excitation has become one of the major issues in TERS. Only low-dimensional materials, e.g., carbon nanotubes, fullerenes, and thin films, are commonly studied by TERS, and examination of bulk samples is still a challenging task for the TERS technique.

4. APPLICATION OF NEAR-FIELD RAMAN SPECTROSCOPY

In the previous section, a brief discussion of near-field Raman has been presented for its feasibility in the vibrational spectroscopy at the nanoscale. Although the near-field Raman signal is extremely weak, as estimated in Table 1, researchers managed to obtain the near-field Raman spectra with an unprecedented spatial resolution of important sample systems using aperture tips, including inorganic crystals, polymer thin films, surface-enhanced Raman scattering (SERS) substrates, and liquid–liquid interfaces. Many new phenomena distinct from conventional far-field Raman spectroscopy were found.

4.1. Nonresonant Near-Field Raman Detection of Inorganic Materials

In the past decades, AT-NFRS has been successfully used to characterize chemical and optical properties of many inorganic materials, such as the potassium titanyl phosphate (KTP) crystal,⁷² Si/SiO₂-based samples,^{20,73–75} and diamond.^{51,66,76}

The first AT-NFRS measurement was performed on Rb-doped KTP crystal, a widely used nonlinear optical material, by Jahncke et al. using Al-coated tapered optical fibers.⁷² With its strong Raman response and doping tunability, KTP crystal was considered an excellent candidate for nano-Raman investigations. Jahncke et al. showed that the intensity of the vibrational mode at 767 cm^{−1} was almost doubled in the Rb-doping region in comparison with the KTP bulk, as shown in Figure 7. The

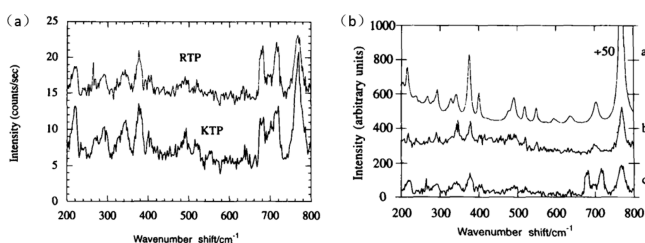


Figure 7. (a) Near-field Raman spectra from the KTP and the rubidium titanyl phosphate (RTP) regions of the sample. The noise of these spectra is 1.1 counts/s. (b) Three Raman spectra on the KTP crystal obtained with the same spectrometer and detector as shown in panel a: (spectrum a) micro-Raman spectrum taken with a conventional optical microscope, (spectrum b) Raman spectrum taken by the SNOM with the fiber probe in the far-field, and (spectrum c) near-field Raman spectrum. For all spectra the excitation source was an argon ion laser with a wavelength of 514.5 nm. Reproduced with permission from ref 72. Copyright 1996 John Wiley and Sons.

enhancement of this vibration mode was explained as the localized stress induced by the Rb-doping effect. In comparison with the far-field micro-Raman that was measured in exactly the same experimental environment, the near-field optical feature, such as the Rayleigh tail, was also observed.⁷²

Other types of popular samples in early near-field Raman studies were Si- and SiO₂-based samples.^{20,73–75} For example, Grausem et al. measured the AT-NFRS spectra of a square grid of SiO₂ dots on a Si substrate using an Al-coated tapered tip. The characteristic Si vibrational mode at 523 cm^{−1} was recorded in this near-field spectrum. When the SNOM tip was moved from the Si substrate to a SiO₂ dot which was 100 nm thick, the near-field Raman scattering from the Si substrate disappeared. This provided a direct proof for the subwavelength resolution of AT-NFRS in the z-direction.⁷³ In comparison with the far-field Raman spectrum, for that obtained by micro-Raman spectroscopy, the near-field Si vibrational mode displays an asymmetric profile, 7 cm^{−1} for the half-width of the low-wavenumber side and 11 cm^{−1} for the half-width of the high-wavenumber side. The spectrum also presented a Raman shift of 10 cm^{−1}. The results imply that the dominant contribution of the Raman signals comes from the crystalline unit cells close to the surface, where the stress is much less than for those in the bulk Si.⁷³

Efforts were also made to study local mechanical stresses in Si wafers using the AT-NFRS technique. For instance, Webster et al. measured the near-field Raman spectra of a damaged Si sample with a scratch in the Si(001) surface, approximately 2

μm wide and 100 μm long, as shown in Figure 8a.⁷⁵ The intensity of the Si Raman mode decreased when the SNOM tip

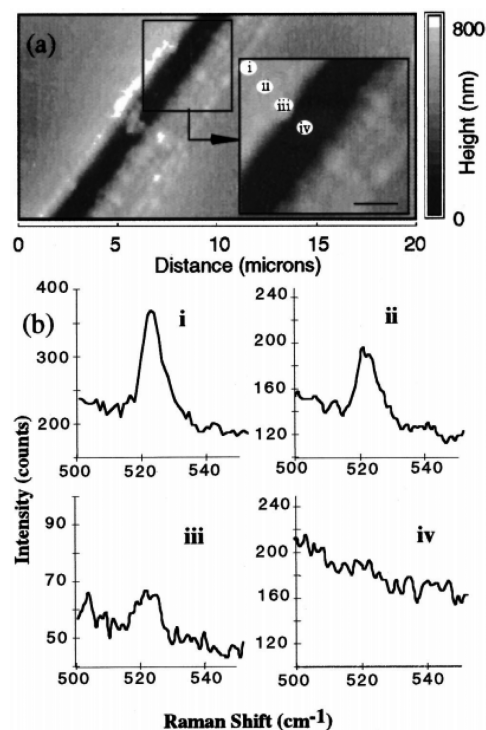


Figure 8. (a) Topography image of the scratched Si sample. The inset is an enlargement of the area of near-field Raman mapping; the scale bar is 1 μm, and labels i–iv indicate locations from which Raman spectra in panel b were obtained. (b) Near-field Raman spectra obtained from points i–iv by using AT-NFRS with 60 s integration time under 633 nm laser excitation. Reproduced with permission from ref 75. Copyright 1998 AIP Publishing LLC.

approached the scratch edge, and the signal finally disappeared when the tip moved into the scratch (Figure 8b). This decrease of the near-field Raman intensity was explained as the result of the phase transformation induced by the high pressure during the scratching. Meanwhile, the Raman mode shifting was observed to be a function of the distance from the scratch, which indicated the compressive stress in the Si substrate.

The scratch directly on the SiO₂ surface was also investigated using AT-NFRS, where the near-field Raman was measured 5 h after the scratching.⁷⁴ Different from the previous work,⁷⁵ where no Raman signal was detected for the scratched Si due to the stress, the freshly grown SiO₂ with a Raman peak at 500 cm^{−1} and the Si Raman mode at 519.7 cm^{−1} were observed.

AT-NFRS was also used to study Raman scattering from other semiconductors, for example, the longitudinal optical (LO) phonon of ZnSe and GaP crystals.⁶⁶ Figure 9a–c shows Raman spectra of a (110)-oriented GaP single crystal under 514 nm laser excitation, revealing the transverse optical (TO) mode at 365 cm^{−1}.⁶⁶ Both far-field and near-field Raman spectra obtained with uncoated and Al-coated tips were plotted and compared in detail. A significant background from Raman scattering was exhibited for the case of uncoated tip in the range up to 500 cm^{−1}, which was explained as light leakage from the side wall of the optical fiber. This background noise was eliminated when the tip was coated by the Al.

Besides traditional semiconductors, many AT-NFRS works were focused on bulk and CVD-grown diamond.^{51,66,76} With its

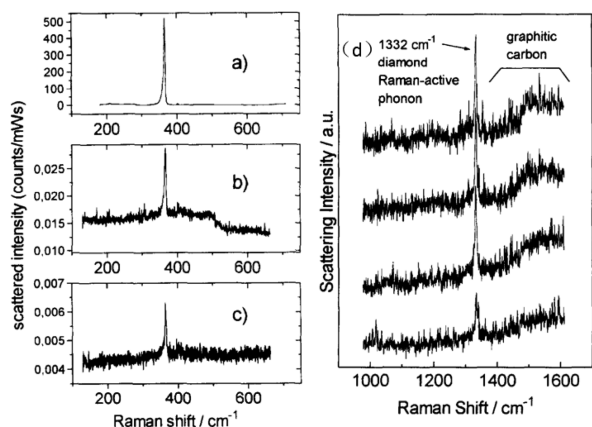


Figure 9. Raman spectra obtained from a GaP(110) surface (a) with conventional micro-Raman and a 100× (0.95 NA) objective lens, (b) with AT-NFRS but employing an uncoated optical fiber tip, and (c) with AT-NFRS and an Al-coated tip. The excitation wavelength was 514.5 nm, and the incident power was 20 mW for panel a and 50 mW for panels b and c. (d) Near-field Raman spectra of CVD-grown diamond and graphitic carbon at different positions on the sample. The averaging recording time was between 30 min and 1 h.⁶⁶ Reproduced with permission from ref 66. Copyright 1998 Elsevier.

high structure symmetry and simple chemical composition, bulk diamond shows only one Raman mode at 1332 cm⁻¹. On the contrary, in the case of grown diamonds, a broad background signal from 1200 to 1600 cm⁻¹ was observed due to the existence of graphitic carbon, as shown in Figure 9.⁶⁵ The near-field Raman results also show that the ratio of carbon to diamond contributions seriously depends on the sample positions (Figure 9d), whereas only weak variation of carbon to diamond ration could be observed with the far-field micro-Raman spectroscopy that was also performed at various positions on the same sample. This result directly demonstrated the capability of the AT-NFRS technique for nanoscale analysis.

A polishing diamond with a uniform and highly stable surface was further investigated by using a specially designed AT-NFRS system.⁷⁷ Figure 10a shows the schematic of the instrument. Al-coated, tapered, optical fiber probes were used for the illumination. The shear-force signal provided a topographic image of the surface as shown in Figure 10b. Transmitted light was collected by an objective lens above the sample, and the reflected light was collected with a combination of an ellipsoidal mirror and a second objective lens. The near-field Raman spectra of the diamond crystal surface for the transmission and reflection measurements are shown in Figure 10c,d. Besides the diamond Raman mode at 1332 cm⁻¹, new features at lower wavenumbers that corresponds to the SiO_x Raman scattering generated from the SNOM optical fiber were also detected in the transmission. This Raman spectral difference can be explained as the radiation from the SNOM tip being asymmetrically distributed in the transmission and forward direction, while the Raman scattered light from the sample is nominally symmetrically distributed between forward and backward directions.

Figure 10e,f shows the dependence between near-field Raman intensity and the tip-sample distance. With the tip-sample distance increasing, the detected Raman intensity rapidly decreased and almost disappeared. This loss of signal with increasing distance is a specific character for the near-field optics, where the near-field from an aperture tip decays

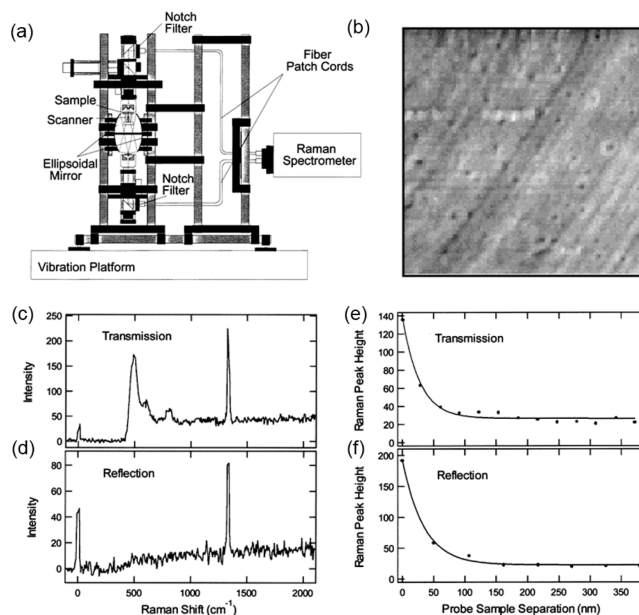


Figure 10. (a) Schematic of the SNOM for the simultaneous acquisition of the transmission and reflection AT-NFRS signal. (b) Topographic image of the diamond crystal surface. (c, d) Near-field Raman spectra of a diamond crystal (~100 nm thickness) recorded by SNOM in transmission and reflection mode. (e, f) Dependence of the diamond Raman intensity at 1332 cm⁻¹ on the tip-to-sample distance for the SNOM transmission and reflection mode. The excitation wavelength for all of the experiments was 488 nm, and the integration time was 5 min. Reproduced with permission from ref 77. Copyright 1999 Elsevier.

exponentially with a characteristic length given by its lateral dimensions. The solid lines in Figure 10e,f are exponential fits to the data for the transmitted and reflected Raman measurements, which are consistent with the near-field decay measured with an aperture probe by Obermüller et al. in the previous work.⁷⁸

4.2. Near-Field Resonant Raman Scattering

AT-NFRS was also used to characterize the resonant Raman scattering from organic materials, especially polymers exhibiting resonant Raman scattering.^{21,79–83} In 1995, Smith et al. performed the first molecular near-field Raman experiment with a subwavelength aperture probe by using the shear-force feedback.²¹ With the improved stability of the instrument, the polydiacetylene (PDA) molecule was first to be used for resonant Raman signal detection under an excitation laser of 633 nm.⁸⁰

PDA molecules with different sizes from a few hundred nanometers to several micrometers dispersed on a glass slide were measured by AT-NFRS with an Al-coated optical fiber probe. Figure 11a,b shows the resonant near-field Raman spectra of the PDA molecule with its characteristic vibration modes at 1465 and 1485 cm⁻¹. The near-field line scan indicated that the width of this molecule was about 600 nm, which was slightly wider than the estimation made from the confocal microscope inspection. At the same time, the preresonance Raman scattering of the polyphenylenevinylene (PPV) film was also investigated, as shown in Figure 11c. The background signal was mainly due to the 675 nm excitation laser, which can introduce strong autofluorescence from the sample. The near-field Raman scattering could be effectively improved when the excitation laser was changed to 850 nm.²¹

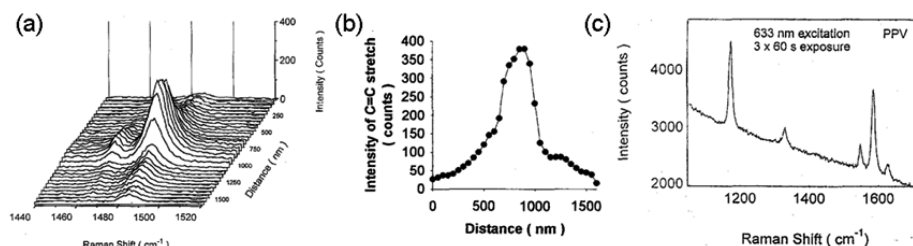


Figure 11. (a) Resonant near-field Raman spectra of a PDA molecule as a function of the positions on the sample. Each spectrum took 30 s to acquire. (b) The intensity of the 1485 cm^{-1} shift of the spectrum in panel a as a function of position across the PDA molecule. The excitation wavelength was 633 nm. (c) A preresonance Raman spectrum of a PPV thin film. Each PPV spectrum took 60 s to acquire. Reproduced with permission from ref 21. Copyright 1995 Elsevier.

AT-NFRS with subwavelength resolution ($\sim 120\text{ nm}$) was further used on organic thin films of tetracyanoquinodimethane (TCNQ).⁸⁴ This TCNQ film can be considered as an efficient Raman scatterer with a strong electron acceptor, and it forms a variety of charge-transfer complexes with inorganic and organic donors.⁸⁴ Figure 12a is the near-field Raman scattering image of

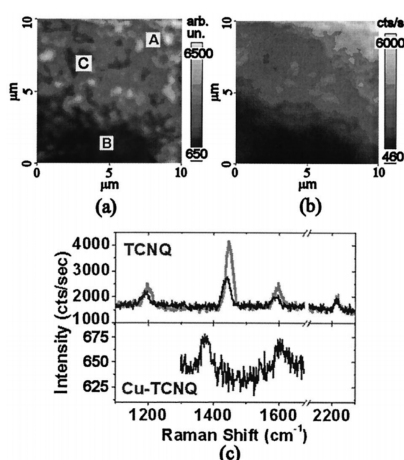


Figure 12. (a) Elastic and (b) Raman scattering map at 1453 cm^{-1} acquired on a border between a TCNQ area (indicated with A and C) and a Cu-TCNQ cluster (indicated with B). The Raman spectra, shown in the top plot of panel c, were acquired respectively at positions A (light gray curve) and C (black curve). They displayed the typical TCNQ peaks with different intensities superimposed onto a constant background. In the spectrum acquired at position B (bottom plot of panel c), the shift of the 1453 cm^{-1} peak toward 1381 cm^{-1} was observed, representing the chemical fingerprint of the Cu-TCNQ compound. The TCNQ Raman spectrum was obtained with an excitation power of $\sim 100\text{ nW}$ and an integration time of 300 ms per point, while the Cu-TCNQ spectrum required an integration time of 5 s per point to evidence the frequency shift with an appreciable signal-to-noise ratio. The excitation wavelength for all the experiments was 514.5 nm . Reproduced with permission from ref 84. Copyright 2003 The Optical Society.

the TCNQ film, where the darker area (position B) shows that the signal was attenuated in comparison with positions A and C. This Raman intensity change indicated the presence of a strongly absorbing material, such as the Cu-TCNQ aggregates, which was verified by the vanishing of the Raman activity at 1453 cm^{-1} in position B (Figure 12b). Near-field Raman spectra were acquired on sites A and B (Figure 12c). The spectrum of site A displayed the chemical fingerprint of the neutral TCNQ with the most intense peaks at 1453 cm^{-1} (C=C wing stretching), 1196 cm^{-1} (C=C-H bending), 1600

cm^{-1} (C=C ring stretching), and 2221 cm^{-1} (C≡N stretching) superimposed onto an elastic stray light background. A clear shift of the 1453 cm^{-1} peak toward 1381 cm^{-1} was found in the position B spectrum, proving the occurrence of salt in this area. For the spectrum of position C, the background baseline remained the same as the one of position A but with an obvious intensity change for the Raman peak at 1453 cm^{-1} .

4.3. Near-Field Study of SERS Using Aperture Tips

In addition to applications in material science, the subwavelength spatial resolution of SNOM makes it a powerful tool for investigating important nano-optical phenomena, e.g., SERS. In SERS, nanostructured metallic substrates are used as an antenna to enhance the excitation and emission process of Raman scattering.²² Its mode intensity, polarization, and selection rule are highly dependent on the local geometry because of the localized surface plasmon resonances.³⁷ By combining aperture SNOM with SERS, the spectral, spatial, and chemical information on organic molecules, as well as the topology of the substrates, can be obtained simultaneously with a subwavelength lateral resolution. This provides valuable information for understanding the mechanism of SERS phenomena.^{81–83}

To demonstrate the capability of AT-NFRS, the SERS spectra of Rhodamine 6G (R6G) and cresyl fast violet (CFV) on Ag substrates were measured using AT-NFRS with a short exposure time and a larger signal-to-noise ratio.^{81,82} The dependence of the Raman enhancement on the substrate morphology was revealed. The weakest Raman signal was recorded on a 500-nm-sized Ag particle (position C), whereas the maximum SERS intensities were found over or between a number of small Ag nanoparticles, as shown in positions A and B of Figure 13. This strong spatial variation of the SERS intensities indicates: (i) a reflectivity difference due to the local topography; (ii) concentration variations of the tested molecules, and (iii) localized Raman variations due to the specific environment.

To understand the origin of the “hot spots” in single-molecule SERS, Emory and Nie measured the near-field Raman spectra of single Ag colloidal nanoparticles with excitation intensities as low as 10 nW using AT-NFRS with an Al-coated fiber probe.⁸³ As shown in Figure 14a–d, the Raman signals of R6G molecule at 1653 , 1570 , 1513 , 1363 , 1314 , and 1183 cm^{-1} arise from the symmetric in-plane C–C stretching vibration modes that were resonance-enhanced under 514 nm laser excitation. A direct comparison of the near-field and confocal results shows that near-field optical excitation did not lead to significantly different selection rules in Raman spectroscopy. This is an advantage of the aperture SNOM in comparison with

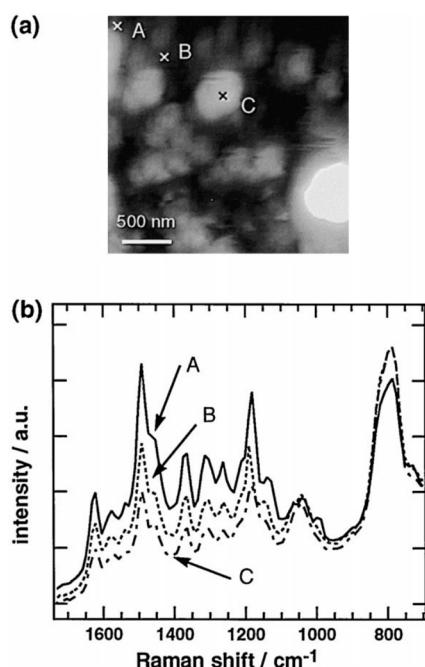


Figure 13. (a) AFM image of the CFV sample with three marked points, A–C, and (b) near-field SERS spectra of CFV on a Ag substrate recorded at corresponding positions A–C. The sample stage drift was 50 nm/image, and the spectral resolution was less than 10 cm^{-1} . The incident laser wavelength was 514 nm, and the exposure time of the CCD camera was 100 s. Reproduced with permission from ref 81. Copyright 1998 Elsevier.

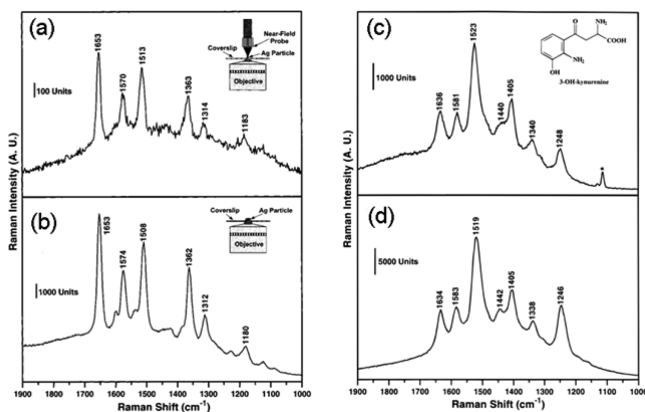


Figure 14. (a, c) Near-field and (b, d) confocal surface-enhanced Raman spectra of R6G and 3-hydroxykynurenine molecules adsorbed on a single Ag nanoparticle. The incident laser wavelength was 514.5 nm, and the laser power was 10 nW (a), 2.5 μW (b), 30 nW (c), and 0.4 μW (d). The integration time for the Raman measurements was 30 s (a), 10 s (b), 10 s (c), and 60 s (d). Reproduced from ref 83. Copyright 1997 American Chemical Society.

the apertureless one (TERS), where different Raman selection rules may be expected in the near-field because of the complex tip–sample interactions and the presence of a significant z -component in the electromagnetic field at the tip periphery.⁸³

To understand the SERS phenomena further, Anger et al. measured the SERS spectra of R6G molecules on Ag nanoclusters using low-temperature aperture-SNOM.¹⁶ Near-field Raman spectra from room temperature down to 8.5 K were recorded. At 8.5 K, the enhanced Raman spectra of R6G exhibited a much higher signal-to-noise ratio than in the case of

room temperature. Lines at 524, 460, and 405 cm^{-1} , corresponding to torsional and flexural modes of the xanthen structure of the R6G molecules, clearly appeared, while these Raman lines could not be easily seen at the room temperature because of the fluorescence background. In addition, with the decreasing of the measurement temperature from 300 to 8.5 K, an anti-Stokes line was found to be shifted and finally vanished when the sample was cooled down. This is because the population of the excited state of the vibrational modes decreases with temperature.

In the same work, Anger et al. also correlated the low-temperature near-field SERS with the topology of the sample.¹⁶ They mapped the Raman spectra of a R6G molecule across an Ag cluster at 77 K. One can see the change from fluorescence toward the Raman signal of the dye molecules within the Ag cluster. This can be explained by the quenching effect of the Ag cluster.

4.4. Near-Field Raman Spectroscopy at Liquid–Liquid Interfaces

Besides solid-state samples, AF-NFRS can also be applied to liquid samples. As discussed in section 3, one of the biggest advantages of an aperture-SNOM system is the small excitation volume, which allows AF-NFRS to excite the sample locally without introducing background from the environment. This unique property makes AF-NFRS a powerful tool for analyzing low-dimensional systems in liquid environments that are difficult for other analytical methods due to the background issue.⁸⁵

One such system is liquid–liquid interfaces, which play an important role in physics, chemistry, and biology.^{86,87} To filter out Raman signals generated at the interface from the background generated by bulk solutions, De Serio et al. developed an AT-NFRS-based system and investigated the Raman spectra of liquid–liquid interfaces with subwavelength spatial resolution.^{60,86} The AT-NFRS system for interface investigation is shown in Figure 15. Near-field excitation was

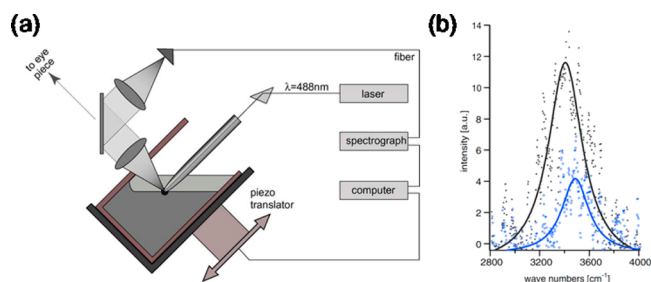


Figure 15. Near-field Raman spectroscopy of a liquid–liquid (CCl_4 – H_2O) interface. (a) Schematic of the setup. (b) Change of the Raman water band. The black curve and blue curve were the measured water band before and after the tip reached the interface, respectively. Reproduced with permission from ref 60. Copyright 2006 Elsevier.

used. The 488 nm line of an argon laser (2.5 mW) was coupled to the metalized fiber tip (100 nm aperture), and the Raman signals were collected in the far-field. During measurements, the tip was fixed and the liquid–liquid interface was moved across the tip apex using a piezo-stage. Because the excitation field only extended for tens of nanometers in theory, one should be able to see the signal from the interface. Indeed, in this work, a blue shift of the O–H stretching mode was observed at the interface (Figure 15b), implying a weakening of the intermolecular interactions at the interface.

Though only how Raman signals change in the direction normal to the interface was investigated, the results shows the potential of AT-NFRS for investigating interfaces or membrane systems in liquid environments.

5. RECENT ADVANCES IN TIP DESIGN

From the above discussions of the applications of near-field Raman, although the AT-NFRS technique had some successes, after 2000, the number of publications on aperture-SNOM dropped abruptly and people's interest shifted to apertureless-SNOM techniques because of the relatively poor spatial resolution and low signal intensity of conventional aperture-SNOM. Meanwhile, after 2000, other nano-optics-related areas experienced a rapid growth, and new concepts, such as plasmonic nanoantennas, extraordinary transmission, and metasurfaces, were reported. This brings a lot of new opportunities to the field of aperture-SNOM. In this part, we review those new developments in the context of attaining high-performance aperture-SNOM.

5.1. Extraordinary Transmission

In parallel to the development of aperture-SNOM, Ebbesen and co-workers⁸⁸ demonstrated that the transmission of subwavelength apertures can be increased due to the excitation of surface plasmon polaritons (SPPs) when a periodic arrangement was used. This idea was later extended to the case of a single subwavelength nanoaperture by Lezec and co-workers.^{89,90} They demonstrated that with nanofabricated gratings, the transmission and directivity of light can be improved dramatically (Figure 16a). With the enhanced

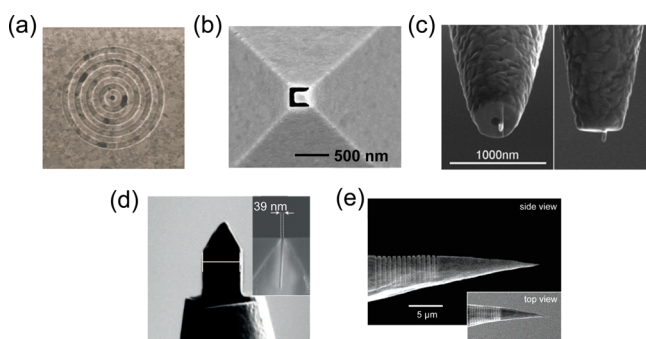


Figure 16. (a) The SEM image of a plasmonic nanoaperture surrounded by gratings, which exhibits an extraordinary transmission effect. Reproduced with permission from ref 90. Copyright 2002 The American Association for the Advancement of Science. (b) C-shaped antenna probe. Reproduced with permission from ref 95. Copyright 2013 Nature Publishing Group. (c) Monopole antenna on the top of an aperture probe. Reproduced from ref 39. Copyright 2007 American Chemical Society. (d) Side view of the campanile-style tip. The inset shows the nanometer gap at the tip apex. Reproduced with permission from ref 97. Copyright 2012 The American Association for the Advancement of Science. (e) SEM image of a fabricated grating-coupled plasmonic tip. Reproduced from ref 98. Copyright 2007 American Chemical Society.

transmission, Brolo et al.⁹¹ demonstrated surface-enhanced Raman spectroscopy using periodic nanoholes. In the future, it would be interesting to use this phenomenon to improve the performance of aperture tips.

5.2. Nanostructured Aperture Tips

In 1990s, Pohl and other researchers pointed out that the SNOM tip is an optical antenna.⁹² This idea did not gain much

attention until a decade later, when plasmonic nanoantenna emerged as a new research field. Inspired by the nanoparticle-based antennas,^{93,94} attempts were made to use subwavelength aperture antennas to improve the light coupling efficiency and enhance the local light intensity. Typical designs include the C-shaped aperture (Figure 16b), bow-tie-shaped aperture, and nanohole pair.^{95,96} These designs provide high local field intensity and lead to extreme light confinement, which has been demonstrated as efficient for trapping and detecting nanoparticles and even single molecules.

Although the aperture antennas are capable of creating large field enhancement, it is difficult to use them as SNOM tips because the electric fields are normally localized inside the aperture and cannot be used to excite the sample efficiently. Interestingly, in SNOM measurements, people found that the nanometer roughness of the metal coating on the tip apex often gave unexpectedly strong signals due to the lightning rod effect of small local protrusions. Using this principle, Keilmann and co-workers grew a tiny metal tip on the side of a nanoaperture to draw the field out of the aperture and form a large local field enhancement at the apex of the metal tip.⁹⁹ With this type of hybrid tip, a single-molecule fluorescence image with 25 nm resolution was obtained. Later, this idea was further developed by van Hulst and co-workers, who showed that when the additional metal probe reached the resonance condition with the excitation wavelength, the local light intensity under the tip apex could be enhanced by 3 orders of magnitude (Figure 16c).³⁹ Considering 1 μ W of laser coupled out of the aperture (100 nm in diameter), g^4 is approximately 10^6 times and V_{exc} is $25 \times 25 \times 10$ nm, so the Raman power of a pure sample is approximately 10^{-15} W, which is comparable to the signal strength of a conventional TERS measurement (Table 1).

Another promising design of the aperture-antenna tip is the campanile-style tip reported by Bao et al.^{97,100} As shown in Figure 16d, the campanile uses a pair of opposite triangular Au films to squeeze the light into a 40 nm area with 2 orders of magnitude field enhancement at the tip top. To some extent, it can be treated as a 3D bow-tie antenna with the two arms folded into a waveguide. Using eq 6, we can estimate the intensity of the Raman signal for this hybrid resonant probe, and it is 6 orders higher than the conventional probe, making it an attractive candidate for nano-Raman measurements.

5.3. Plasmonic-Waveguide-Based Near-Field Tip

The essence of aperture-SNOM is to use a waveguide to deliver and confine the photons into the nanoscale without the far-field excitation-induced background, which is suffered by the apertureless-SNOM technique.^{61,101,102} It is therefore interesting to use a tapered plasmonic waveguide instead of a tapered fiber to confine light into the nanoscale. Because of the large spatial frequency k and no need for a physical aperture, plasmonic-waveguide-based near-field probes offers much better spatial resolution and a higher power transmission efficiency, which are crucial for nano-Raman mapping.

Interestingly, the above-described design principle can be found in one of the earliest types of SNOM tips, the metal-coated tetrahedral tips created by Fisher and co-workers. With the help of the tetrahedral tip, Raman mapping with a 30 nm spatial resolution was demonstrated.^{103,104} Later, Oh and co-workers developed a microfabrication-based technique that allowed the mass production of high-quality pyramid tips with a high yield.¹⁰⁵ Another example belonging to this category is the grating-coupled plasmonic tip reported by Raschke and co-

workers (Figure 16e).⁹⁸ Using an optimized Au tip, they were able to localize the light into an area of ~ 10 nm with 10^5 -fold enhancement.

6. PERSPECTIVE

In the last couple of decades, driven by the rapid growth of nanoscience and nanotechnology, many near-field optical techniques have been developed for nanoscale analysis, including AT-NFRS,⁵¹ TERS,^{25,33} and nano-IR techniques.^{28,106–108} In this review, we focus on the AT-NFRS technique and cover the historical development of the instrumentation and applications of the AT-NFRS technique with the emphasis on its advantages and limitations. Although the signal intensity and spatial resolution of the AT-NFRS did not reach researchers' original expectations and fewer results were published after 2000, its small excitation volume and the consequent low background make the aperture-tip technique still feasible for many important samples that cannot be measured with other optical nanospectroscopy methods. Moreover, recent progress shows that the power transmission efficiency and local field intensity supported by aperture tips can be significantly improved by using new tip designs. From this prospect, we think that there is still much room for the development of the aperture-SNOM-based Raman technique.

Indeed, driven by the rapid advances in the field of plasmonics and nanofabrication techniques, aperture-SNOM is experiencing a renaissance, with new aperture tips or related plasmonic designs reported frequently. An inspiring example is the hybrid structure of aperture and bowtie antenna demonstrated by Ahmed and Gordon.^{109,110} In their work, a plasmonic dipole antenna was placed at the center of a nanoaperture, which reduced the detection volume and depressed the background significantly. Another important example is the aperture–rod hybrid SNOM tip, reported by van Hulst and co-workers, discussed in section 5.³⁹ It will be interesting to see this design principle be used for new aperture-SNOM tips.

In addition to the hybrid design, the plasmonic waveguide-based tip provides another possibility. As discussed in section 5, a large field enhancement can be obtained at the tip apex of a metal tip by focusing the propagating SPPs on the tip surface without using far-field excitations. Compared with the tapered fiber tips, SPPs have a much higher k and can therefore squeeze light into a nanometer scale with a higher efficiency. Currently, this technique was demonstrated on nanostructured conical Au tips, which were difficult to fabricate and tricky to align with the optical system.^{67,98} In the future, it would be interesting to implement the design principle on the SiO_2 pyramid tips, which can potentially be fabricated in a large scale with a high yield¹⁰⁵ and, more importantly, can be integrated with microscope system for rapid and convenient optical alignment.

Another interesting direction for improving the performance of AT-NFRS is to use ultraviolet (UV) excitation light, which has several advantages compared with the visible and near-IR excitation commonly used today. First, the smaller wavelength shifts the cutoff regime in a tapered fiber tip toward its apex and therefore leads to a better power transmission efficiency.²³ Second, the Raman scattering strength is proportional to the fourth power of the excitation frequency, and changing the excitation wavelength to the UV regime can increase the signal by approximately 1 order of magnitude.^{3,4} In addition, in the UV spectral regime, the excitation is resonant with the electronic transition of the majority of organic molecules and

induces a further signal improvement due to the resonant Raman effect (up to 10^6 -fold).²² Encouraged by the advantages above, UV near-field Raman spectroscopy with aperture tips^{111,112} and apertureless tips^{113,114} have been recently demonstrated. Today, low-cost UV laser sources and UV fibers have become broadly available, and one can foresee the wide implementation of UV near-field Raman spectroscopy in the near future.

In this review, the polarization effects at the tip apex have not been discussed, which have become increasingly important in the field of the near-field Raman technique because of the strong polarization dependence of the Raman scattering of low-dimension materials. Indeed, with a well-defined aperture tip, the polarization state can be precisely controlled in the direction parallel to the sample,^{115–117} and this is different from the case of TERS, in which the polarization of the enhanced fields is always perpendicular to the local surface of the tip.

The development of high-performance aperture tips can bring many new applications. One important example is biological samples in a liquid environment, which are extremely challenging for other optical nanospectroscopic techniques (i.e., TERS and nano-IR) because of the huge background. With an aperture tip, there is no such issue because of the extremely small excitation volume in the aperture-SNOM technique.

From our point of view, aperture-SNOM is a powerful platform that possesses unique properties, including its low background level, the feasibility for a broad spectral range (from UV to near-IR), and the capability of polarization control, though its spatial resolution and sensitivity are relatively low today. In the future, with the advances of numerical design and nanofabrication techniques, new high-performance aperture tips may be introduced and lead to a quantum leap in the development of the nano-Raman mapping technique, establishing it as an important tool for nanoscale chemical analysis.

AUTHOR INFORMATION

Corresponding Author

*E-mail: zhyfang@pku.edu.cn.

ORCID

Zheyu Fang: 0000-0001-5780-0728

Notes

The authors declare no competing financial interest.

Biographies

Weihua Zhang is a professor in the College of Engineering and Applied Sciences at Nanjing University (Nanjing, China). He received his M.S. degree in physics at Peking University (Beijing, China) in 2004 and his Ph.D. degree in analytical chemistry at ETH Zurich (Zurich, Switzerland) in 2008, followed by two postdoctoral appointments at École Polytechnique Fédérale de Lausanne (Lausanne, Switzerland) in 2008–2010 and at Princeton University (Princeton, NJ) in 2010–2013. In 2013, he was selected in the 1000 Young Talent Plan of China and joined the faculty at Nanjing University. His research interests include plasmonics, nanofabrication, computational optics, and nanoscale analysis using near-field optical microscopy and spectroscopy.

Zheyu Fang is a professor of physics at Peking University, in Beijing, China. He received his B.S. degree from Nankai University in 2006 and his Ph.D. degree in physics from Peking University with Prof. Xing Zhu, in 2011, followed by a postdoctoral appointment at Rice

University (Houston, TX) with Prof. Naomi J. Halas and Prof. Peter Nordlander (2011–2013). He joined the faculty at Peking University in 2012, and his current research interests are near-field optics, plasmonics, and nanophotonic materials and devices. He has published over 100 original research papers in peer-reviewed, international journals with more than 3000 SCI citations. He was honored with National Excellent Doctoral Dissertation of China (2013), the Excellent Youth Scholars career award of National Science Foundation of China (2014), and also was selected as one of the National Top-Notch Young Professionals of China (2015).

Xing Zhu is professor of physics at Peking University and deputy director of the National Center for Nanoscience & Technology, in Beijing, China. He obtained his M.S. at University of Toronto (Toronto, Canada) in 1983 and Ph.D. in applied physics at University of Saarland (Saarbrücken, Germany) with Prof. Herbert Gleiter. His research areas are the synthesis of nanostructured materials and their characterization and scanning probe microscopy with emphasis on scanning near-field microscopy to study the light–matter interaction at nanometer scale.

ACKNOWLEDGMENTS

This work is supported by the National Key Technologies R&D Program of China (No. 2016YFA0201104), National Basic Research Program of China (973 Program, Grant No. 2015CB932403), and National Science Foundation of China (Grant No. 61422501, 11374023, 11374152, 11674012, 61176120, 61378059, 11574142, 61521004), Beijing Natural Science Foundation (Grant No. L140007), and Foundation for the Author of National Excellent Doctoral Dissertation of China (Grant No. 201420), National Program for Support of Top-Notch Young Professionals, 1000 Young Talent Plan, and the Priority Academic Program Development (PAPD) of Jiangsu Higher Education Institutions.

REFERENCES

- (1) Bradbury, S. *The Evolution of the Microscope*; Pergamon Press Ltd.: London, 1967.
- (2) Schrader, B. *Infrared and Raman Spectroscopy: Methods and Applications*; VCH Publishers: Weinheim, Germany, 1995.
- (3) Winefordner, J. D. *Raman Spectroscopy for Chemical Analysis*; John Wiley & Sons, Inc.: New York, 2000.
- (4) Smith, E.; Dent, G. *Modern Raman Spectroscopy: A Practical Approach*; John Wiley & Sons Ltd: West Sussex, England, 2005.
- (5) Turrell, G.; Corset, J. *Raman Microscopy: Developments and Applications*; Elsevier Ltd.: Gaithersburg, MD, 1996.
- (6) Dieing, T.; Holtricher, O.; Toporski, J. *Confocal Raman Microscopy*; Springer: Heidelberg, Germany, 2010.
- (7) Novotny, L.; Hecht, B. *Principles of Nano-Optics*; Cambridge University Press: New York, 2012.
- (8) Abbe, E. Beiträge zur Theorie des Mikroskops und der mikroskopischen Wahrnehmung. *Archiv für Mikroskopische Anatomie* **1873**, 9, 413.
- (9) Sygne, E. H. A Suggested Method for Extending the Microscopic Resolution into the Ultramicroscopic Region. *Philos. Mag.* **1928**, 6, 356.
- (10) Ash, E. A.; Nicholls, G. Super-Resolution Aperture Scanning Microscope. *Nature* **1972**, 237, 510.
- (11) Binnig, G.; Rohrer, H. Scanning Tunneling Microscopy. *IBM J. Res. Dev* **1981**, 30, 355.
- (12) Lewis, A.; Isaacson, M.; Harootunian, A.; Muray, A. Development of a 500 Å Spatial Resolution Light Microscope. I. Light is Efficiently Transmitted through $\lambda/16$ Diameter Apertures. *Ultramicroscopy* **1984**, 13, 227.
- (13) Pohl, D. W.; Denk, W.; Lanz, M. Optical Stethoscopy: Image Recording with Resolution $\lambda/20$. *Appl. Phys. Lett.* **1984**, 44, 651.
- (14) Betzig, E.; Trautman, J. K.; Harris, T. D.; Weiner, J. S.; Kostelak, R. L. Breaking the Diffraction Barrier - Optical Microscopy on a Nanometric Scale. *Science* **1991**, 251, 1468.
- (15) Betzig, E.; Trautman, J. K. Near-Field Optics - Microscopy, Spectroscopy, and Surface Modification Beyond the Diffraction Limit. *Science* **1992**, 257, 189.
- (16) Anger, P.; Feltz, A.; Berghaus, T.; Meixner, A. Near-Field and Confocal Surface-Enhanced Resonance Raman Spectroscopy at Cryogenic Temperatures. *J. Microsc.* **2003**, 209, 162.
- (17) Zeisel, D.; Dutoit, B.; Deckert, V.; Roth, T.; Zenobi, R. Optical Spectroscopy and Laser Desorption on a Nanometer Scale. *Anal. Chem.* **1997**, 69, 749.
- (18) Stockle, R.; Setz, P.; Deckert, V.; Lippert, T.; Wokaun, A.; Zenobi, R. Nanoscale Atmospheric Pressure Laser Ablation-Mass Spectrometry. *Anal. Chem.* **2001**, 73, 1399.
- (19) Knoll, B.; Keilmann, F. Near-Field Probing of Vibrational Absorption for Chemical Microscopy. *Nature* **1999**, 399, 134.
- (20) Webster, S.; Smith, D.; Batchelder, D. Raman Microscopy Using a Scanning Near-Field Optical Probe. *Vib. Spectrosc.* **1998**, 18, 51.
- (21) Smith, D. A.; Webster, S.; Ayad, M.; Evans, S. D.; Fogherty, D.; Batchelder, D. Development of a Scanning Near-Field Optical Probe for Localised Raman Spectroscopy. *Ultramicroscopy* **1995**, 61, 247.
- (22) Le Ru, E.; Etchegoin, P. *Principles of Surface Enhanced Raman Spectroscopy and Related Plasmonic Effects*; Elsevier: Oxford, Great Britain, 2009.
- (23) Novotny, L.; Hafner, C. Light Propagation in a Cylindrical Waveguide with a Complex, Metallic, Dielectric function. *Phys. Rev. E: Stat. Phys., Plasmas, Fluids, Relat. Interdiscip. Top.* **1994**, 50, 4094.
- (24) Zenhausem, F.; Martin, Y.; Wickramasinghe, H. K. Scanning Interferometric Apertureless Microscopy: Optical Imaging at 10 Angstrom Resolution. *Science* **1995**, 269, 1083.
- (25) Stöckle, R. M.; Suh, Y. D.; Deckert, V.; Zenobi, R. Nanoscale Chemical Analysis by Tip-Enhanced Raman Spectroscopy. *Chem. Phys. Lett.* **2000**, 318, 131.
- (26) Anderson, M. S. Locally Enhanced Raman Spectroscopy with an Atomic Force Microscope (AFM-TERS). *Appl. Phys. Lett.* **2000**, 76, 3130.
- (27) Hayazawa, N.; Inouye, Y.; Sekkat, Z.; Kawata, S. Metallized Tip Amplification of Near-Field Raman Scattering. *Opt. Commun.* **2000**, 183, 333.
- (28) Hillenbrand, R.; Taubner, T.; Keilmann, F. Phonon-Enhanced Light-Matter Interaction at the Nanometer Scale. *Nature* **2002**, 418, 159.
- (29) Keilmann, F.; Hillenbrand, R. Near-Field Microscopy by Elastic Light Scattering from a Tip. *Philos. Trans. R. Soc., A* **2004**, 362, 787.
- (30) Gomez, L.; Bachelot, R.; Bouhelier, A.; Wiederrecht, G. P.; Chang, S.-H.; Gray, S. K.; Hua, F.; Jeon, S.; Rogers, J.; Castro, M. E.; Blaize, S.; Stefanon, I.; Lerondel, G.; Royer, P. Apertureless Scanning Near-Field Optical Microscopy: a Comparison between Homodyne and Heterodyne Approaches. *J. Opt. Soc. Am. B* **2006**, 23, 823.
- (31) Neacsu, C. C.; Dreyer, J.; Behr, N.; Raschke, M. B. Scanning-Probe Raman Spectroscopy with Single-Molecule Sensitivity. *Phys. Rev. B: Condens. Matter Mater. Phys.* **2006**, 73, 193406.
- (32) Zhang, W.; Yeo, B.-S.; Schmid, T.; Zenobi, R. Single Molecule Tip-Enhanced Raman Spectroscopy with Silver Tips. *J. Phys. Chem. C* **2007**, 111, 1733.
- (33) Steidtner, J.; Pettinger, B. Tip-Enhanced Raman Spectroscopy and Microscopy on Single Dye Molecules with 15 nm Resolution. *Phys. Rev. Lett.* **2008**, 100, 236101.
- (34) Jiang, S.; Zhang, Y.; Zhang, R.; Hu, C.; Liao, M.; Luo, Y.; Yang, J.; Dong, Z.; Hou, J. Distinguishing Adjacent Molecules on a Surface using Plasmon-Enhanced Raman Scattering. *Nat. Nanotechnol.* **2015**, 10, 865.
- (35) Zhang, R.; Zhang, Y.; Dong, Z.; Jiang, S.; Zhang, C.; Chen, L.; Zhang, L.; Liao, Y.; Aizpurua, J.; Luo, Y.; Yang, J. L.; Hou, J. G. Chemical Mapping of a Single Molecule by Plasmon-Enhanced Raman Scattering. *Nature* **2013**, 498, 82.

- (36) Yano, T.-a.; Inouye, Y.; Kawata, S. Nanoscale Uniaxial Pressure Effect of a Carbon Nanotube Bundle on Tip-Enhanced Near-Field Raman Spectra. *Nano Lett.* **2006**, *6*, 1269.
- (37) Ayars, E.; Hallen, H. D.; Jahncke, C. Electric Field Gradient Effects in Raman Spectroscopy. *Phys. Rev. Lett.* **2000**, *85*, 4180.
- (38) Hartschuh, A.; Anderson, N.; Novotny, L. Near-Field Raman Spectroscopy Using a Sharp Metal Tip. *J. Microsc.* **2003**, *210*, 234.
- (39) Taminiau, T. H.; Moerland, R. J.; Segerink, F. B.; Kuipers, L.; van Hulst, N. F. $\lambda/4$ Resonance of an Optical Monopole Antenna Probed by Single Molecule Fluorescence. *Nano Lett.* **2007**, *7*, 28.
- (40) Pohl, D. W.; Kawata, S.; Inouye, Y.; Fischer, U. C.; Dereux, A.; Weeber, J.-C.; Hayashi, S.; Okamoto, T.; Novotny, L.; Sugiura, T.; Osawa, M.; Kano, H. *Near-Field Optics and Surface Plasmon Polaritons*; Springer-Verlag: Berlin, 2001.
- (41) Rugar, D.; Mamin, H. J.; Guethner, P. Improved Fiber-Optic Interferometer for Atomic Force Microscopy. *Appl. Phys. Lett.* **1989**, *55*, 2588.
- (42) Toledo-Crow, R.; Yang, P. C.; Chen, Y.; Vaez-Iravani, M. Near-field Differential Scanning Optical Microscope with Atomic Force Regulation. *Appl. Phys. Lett.* **1992**, *60*, 2957.
- (43) Tarrach, G.; Bopp, M. A.; Zeisel, D.; Meixner, A. J. Design and Construction of a Versatile Scanning Near-Field Optical Microscope for Fluorescence Imaging of Single Molecules. *Rev. Sci. Instrum.* **1995**, *66*, 3569.
- (44) Karrai, K.; Grober, R. D. Piezoelectric Tip-Sample Distance Control for Near-Field Optical Microscopes. *Appl. Phys. Lett.* **1995**, *66*, 1842.
- (45) Tsai, D. P.; Lu, Y. Y. Tapping-Mode Tuning Fork Force Sensing for Near-Field Scanning Optical Microscopy. *Appl. Phys. Lett.* **1998**, *73*, 2724.
- (46) Giessibl, F. J. High-Speed Force Sensor for Force Microscopy and Profilometry Utilizing a Quartz Tuning Fork. *Appl. Phys. Lett.* **1998**, *73*, 3956.
- (47) Nony, L.; Barattoff, A.; Schär, D.; Pfeiffer, O.; Wetzel, A.; Meyer, E. Noncontact Atomic Force Microscopy Simulator with Phase-Locked-Loop Controlled Frequency Detection and Excitation. *Phys. Rev. B: Condens. Matter Mater. Phys.* **2006**, *74*, 235439.
- (48) Zhang, J.; Chen, P. C.; Yuan, B. K.; Ji, W.; Cheng, Z. H.; Qiu, X. H. Real-Space Identification of Intermolecular Bonding with Atomic Force Microscopy. *Science* **2013**, *342*, 611.
- (49) Valaskovic, G.; Holton, M.; Morrison, G. Parameter Control, Characterization, and Optimization in the Fabrication of Optical Fiber Near-Field Probes. *Appl. Opt.* **1995**, *34*, 1215.
- (50) Turner, D. R. US Patent 4,469,554, 1984.
- (51) Zenobi, R.; Deckert, V. Scanning Near-Field Optical Microscopy and Spectroscopy as a Tool for Chemical Analysis. *Angew. Chem., Int. Ed.* **2000**, *39*, 1746.
- (52) De Serio, M.; Zenobi, R.; Deckert, V. Looking at the Nanoscale: Scanning Near-Field Optical Microscopy. *TrAC, Trends Anal. Chem.* **2003**, *22*, 70.
- (53) Stöckle, R.; Fokas, C.; Deckert, V.; Zenobi, R.; Sick, B.; Hecht, B.; Wild, U. P. High-Quality Near-Field Optical Probes by Tube Etching. *Appl. Phys. Lett.* **1999**, *75*, 160.
- (54) Pangaribuan, T.; Yamada, K.; Jiang, S.; Ohsawa, H.; Ohtsu, M. Reproducible Fabrication Technique of Nanometric Tip Diameter Fiber Probe for Photon Scanning Tunneling Microscope. *Jpn. J. Appl. Phys.* **1992**, *31*, L1302.
- (55) Eah, S.-K.; Jhe, W.; Arakawa, Y. Nearly Diffraction-Limited Focusing of a Fiber Axicon Microlens. *Rev. Sci. Instrum.* **2003**, *74*, 4969.
- (56) Hecht, B.; Sick, B.; Wild, U. P.; Deckert, V.; Zenobi, R.; Martin, O. J.; Pohl, D. W. Scanning Near-Field Optical Microscopy with Aperture Probes: Fundamentals and Applications. *J. Chem. Phys.* **2000**, *112*, 7761.
- (57) Bethe, H. Theory of Diffraction by Small Holes. *Phys. Rev.* **1944**, *66*, 163.
- (58) Bouwkamp, C. On Bethe's Theory of Diffraction by Small Holes. *Philips Res. Rep.* **1950**, *5*, 321.
- (59) Born, M.; Wolf, E. *Principle of Optics*; Pergamon: New York, 1980.
- (60) De Serio, M.; Mohapatra, H.; Zenobi, R.; Deckert, V. Investigation of the Liquid-Liquid Interface with High Spatial Resolution Using Near-Field Raman Spectroscopy. *Chem. Phys. Lett.* **2006**, *417*, 452.
- (61) Minh, P. N.; Ono, T.; Esashi, M. High Throughput Aperture Near-Field Scanning Optical Microscopy. *Rev. Sci. Instrum.* **2000**, *71*, 3111.
- (62) Naber, A.; Molenda, D.; Fischer, U.; Maas, H.-J.; Höppener, C.; Lu, N.; Fuchs, H. Enhanced Light Confinement in a Near-Field Optical Probe with a Triangular Aperture. *Phys. Rev. Lett.* **2002**, *89*, 210801.
- (63) Raman, C. V. A Change of Wave-Length in Light Scattering. *Nature* **1928**, *121*, 619.
- (64) Raman, C. V.; Krishnan, K. S. A New Type of Secondary Radiation. *Nature* **1928**, *121*, 501.
- (65) Raman, C. V.; Krishnan, K. S. The Optical Analogue of the Compton Effect. *Nature* **1928**, *121*, 711.
- (66) Goetz, M.; Drews, D.; Zahn, D.; Wannemacher, R. Near-Field Raman Spectroscopy of Semiconductor Heterostructures and CVD-Diamond Layers. *J. Lumin.* **1998**, *76-77*, 306.
- (67) Neacsu, C. C.; Berweger, S.; Raschke, M. B. Tip-Enhanced Raman Imaging and Nanospectroscopy: Sensitivity, Symmetry, and Selection Rules. *NanoBiotechnology* **2007**, *3*, 172.
- (68) Kneipp, K.; Moskovits, M.; Kneipp, H. *Surface-Enhanced Raman Scattering*; Springer: Berlin, 2006.
- (69) Maier, S. A. *Plasmonics: Fundamentals and Applications*; Springer Science & Business Media: New York, 2007.
- (70) Vannier, C.; Yeo, B.-S.; Melanson, J.; Zenobi, R. Multifunctional Microscope for Far-Field and Tip-Enhanced Raman Spectroscopy. *Rev. Sci. Instrum.* **2006**, *77*, 023104.
- (71) Zhang, W.; Cui, X.; Martin, O. J. F. Local Field Enhancement of an Infinite Conical Metal Tip Illuminated by a Focused Beam. *J. Raman Spectrosc.* **2009**, *40*, 1338.
- (72) Jahncke, C.; Hallen, H. D.; Paesler, M. Nano-Raman Spectroscopy and Imaging with a Near-Field Scanning Optical Microscope. *J. Raman Spectrosc.* **1996**, *27*, 579.
- (73) Graessem, J. o.; Humbert, B.; Spajer, M.; Courjon, D.; Burneau, A.; Oswalt, J. Near-Field Raman Spectroscopy. *J. Raman Spectrosc.* **1999**, *30*, 833.
- (74) Kaupp, G.; Herrmann, A.; Wagenblast, G. Scanning near-field optical microscopy (SNOM) with uncoated tips. *Proc. SPIE* **1999**, *3607*, 16.
- (75) Webster, S.; Batchelder, D.; Smith, D. Submicron Resolution Measurement of Stress in Silicon by Near-Field Raman Spectroscopy. *Appl. Phys. Lett.* **1998**, *72*, 1478.
- (76) Tsai, D. P.; Othonos, A.; Moskovits, M.; Uttamchandani, D. Raman Spectroscopy Using a Fiber Optic Probe with Subwavelength Aperture. *Appl. Phys. Lett.* **1994**, *64*, 1768.
- (77) Jordan, C. E.; Stranick, S. J.; Cavanagh, R. R.; Richter, L. J.; Chase, D. B. Near-Field Scanning Optical Microscopy Incorporating Raman Scattering for Vibrational Mode Contrast. *Surf. Sci.* **1999**, *433-435*, 48.
- (78) Obermüller, C.; Karrai, K.; Kolb, G.; Abstreiter, G. Transmitted Radiation through a Subwavelength-Sized Tapered Optical Fiber Tip. *Ultramicroscopy* **1995**, *61*, 171.
- (79) Gucciardi, P.; Trusso, S.; Vasi, C.; Patane, S.; Allegrini, M. Nano-Raman Imaging of Cu-TCNQ Clusters in TCNQ Thin Films by Scanning Near-Field Optical Microscopy. *Phys. Chem. Chem. Phys.* **2002**, *4*, 2747.
- (80) Narita, Y.; Tadokoro, T.; Ikeda, T.; Saiki, T.; Mononobe, S.; Ohtsu, M. Near-Field Raman Spectral Measurement of Polydiacetylene. *Appl. Spectrosc.* **1998**, *52*, 1141.
- (81) Zeisel, D.; Deckert, V.; Zenobi, R.; Vo-Dinh, T. Near-Field Surface-Enhanced Raman Spectroscopy of Dye Molecules Adsorbed on Silver Island Films. *Chem. Phys. Lett.* **1998**, *283*, 381.

- (82) Prikulis, J.; Murty, K.; Olin, H.; Käll, M. Large-Area Topography Analysis and Near-Field Raman Spectroscopy Using Bent Fibre Probes. *J. Microsc.* **2003**, *210*, 269.
- (83) Emory, S. R.; Nie, S. Near-Field Surface-Enhanced Raman Spectroscopy on Single Silver Nanoparticles. *Anal. Chem.* **1997**, *69*, 2631.
- (84) Gucciardi, P. G.; Trusso, S.; Vasi, C.; Patanè, S.; Allegrini, M. Optical Near-Field Raman Imaging with Subdiffraction Resolution. *Appl. Opt.* **2003**, *42*, 2724.
- (85) Friedbacher, G.; Bubert, H. *Surface and Thin Film Analysis*; Wiley-VCH Verlag & Co. KGaA: Weinheim, Germany, 2011.
- (86) De Serio, M.; Bader, A. N.; Heule, M.; Zenobi, R.; Deckert, V. A Near-Field Optical Method for Probing Liquid-Liquid Interfaces. *Chem. Phys. Lett.* **2003**, *380*, 47.
- (87) Perera, J. M.; Stevens, G. W. Spectroscopic Studies of Molecular Interaction at the Liquid-Liquid Interface. *Anal. Bioanal. Chem.* **2009**, *395*, 1019.
- (88) Ebbesen, T. W.; Lezec, H. J.; Ghaemi, H.; Thio, T.; Wolff, P. Extraordinary Optical Transmission through Sub-wavelength Hole Arrays. *Nature* **1998**, *391*, 667.
- (89) Lezec, H.; Thio, T. Diffracted Evanescent Wave Model for Enhanced and Suppressed Optical Transmission through Subwavelength Hole Arrays. *Opt. Express* **2004**, *12*, 3629.
- (90) Lezec, H. J.; Degiron, A.; Devaux, E.; Linke, R.; Martin-Moreno, L.; Garcia-Vidal, F.; Ebbesen, T. Beaming Light from a Subwavelength Aperture. *Science* **2002**, *297*, 820.
- (91) Brolo, A. G.; Arctander, E.; Gordon, R.; Leathem, B.; Kavanagh, K. L. Nanohole-Enhanced Raman Scattering. *Nano Lett.* **2004**, *4*, 2015.
- (92) Zhu, X.; Ohtsu, M. *Near-Field Optics: Principles and Applications*; World Scientific: Beijing, 2000.
- (93) Fromm, D. P.; Sundaramurthy, A.; Schuck, P. J.; Kino, G.; Moerner, W. E. Gap-Dependent Optical Coupling of Single "Bowtie" Nanoantennas Resonant in the Visible. *Nano Lett.* **2004**, *4*, 957.
- (94) Mühlischlegel, P.; Eisler, H.-J.; Martin, O. J. F.; Hecht, B.; Pohl, D. W. Resonant Optical Antennas. *Science* **2005**, *308*, 1607.
- (95) Lindquist, N. C.; Johnson, T. W.; Nagpal, P.; Norris, D. J.; Oh, S.-H. Plasmonic Nanofocusing with a Metallic Pyramid and an Integrated C-Shaped Aperture. *Sci. Rep.* **2013**, *3*, 1857.
- (96) Berthelot, J.; Ćimović, S. S.; Juan, M. L.; Kreuzer, M. P.; Renger, J.; Quidant, R. Three-Dimensional Manipulation with Scanning Near-Field Optical Nanotweezers. *Nat. Nanotechnol.* **2014**, *9*, 295.
- (97) Bao, W.; Melli, M.; Caselli, N.; Riboli, F.; Wiersma, D. S.; Staffaroni, M.; Choo, H.; Ogletree, D. F.; Aloni, S.; Bokor, J.; Cabrini, S.; Intonti, F.; Salmeron, M. B.; Yablonovitch, E.; Schuck, P. J.; Weber-Bargioni, A. Mapping Local Charge Recombination Heterogeneity by Multidimensional Nanospectroscopic Imaging. *Science* **2012**, *338*, 1317.
- (98) Ropers, C.; Neacsu, C.; Elsaesser, T.; Albrecht, M.; Raschke, M.; Lienau, C. Grating-Coupling of Surface Plasmons onto Metallic Tips: a Nanoconfined Light Source. *Nano Lett.* **2007**, *7*, 2784.
- (99) Frey, H. G.; Keilmann, F.; Kriele, A.; Guckenberger, R. Enhancing the Resolution of Scanning Near-Field Optical Microscopy by a Metal Tip Grown on an Aperture Probe. *Appl. Phys. Lett.* **2002**, *81*, 5030.
- (100) Bao, W.; Staffaroni, M.; Bokor, J.; Salmeron, M. B.; Yablonovitch, E.; Cabrini, S.; Weber-Bargioni, A.; Schuck, P. J. Plasmonic Near-Field Probes: a Comparison of the Campanile Geometry with Other Sharp Tips. *Opt. Express* **2013**, *21*, 8166.
- (101) Wiederhecker, G.; Cordeiro, C. M. d. B.; Couny, F.; Benabid, F.; Maier, S.; Knight, J.; Cruz, C.; Fragnito, H. Field Enhancement within an Optical Fibre with a Subwavelength Air Core. *Nat. Photonics* **2007**, *1*, 115.
- (102) Dunn, R. C. Near-Field Scanning Optical Microscopy. *Chem. Rev.* **1999**, *99*, 2891.
- (103) Fischer, U. C.; Koglin, J.; Fuchs, H. The Tetrahedral Tip as a Probe for Scanning Near-Field Optical Microscopy at 30 nm Resolution. *J. Microsc.* **1994**, *176*, 231.
- (104) Bortchagovsky, E. G.; Fischer, U. C. A Tetrahedral Tip as a Probe for Tip-Enhanced Raman Scattering and as a Near-Field Raman Probe. *J. Raman Spectrosc.* **2009**, *40*, 1386.
- (105) Johnson, T. W.; Lapin, Z. J.; Beams, R.; Lindquist, N. C.; Rodrigo, S. G.; Novotny, L.; Oh, S.-H. Highly Reproducible Near-Field Optical Imaging with Sub-20-nm Resolution Based on Template-Stripped Gold Pyramids. *ACS Nano* **2012**, *6*, 9168.
- (106) Hammiche, A.; Bozec, L.; Pollock, H. M.; German, M. J.; Reading, M. Progress in Near-Field Photothermal Infrared Microspectroscopy. *J. Microsc.* **2004**, *213*, 129.
- (107) Amenabar, I.; Poly, S.; Nuansing, W.; Hubrich, E. H.; Govyadinov, A. A.; Huth, F.; Krutokhvostov, R.; Zhang, L. B.; Knez, M.; Heberle, J.; Bittner, A. M.; Hillenbrand, R. Structural Analysis and Mapping of Individual Protein Complexes by Infrared Nanospectroscopy. *Nat. Commun.* **2013**, *4*, 2890.
- (108) Lu, F.; Jin, M. Z.; Belkin, M. A. Tip-Enhanced Infrared Nanospectroscopy via Molecular Expansion Force Detection. *Nat. Photonics* **2014**, *8*, 307.
- (109) Ahmed, A.; Gordon, R. Single Molecule Directivity Enhanced Raman Scattering Using Nanoantennas. *Nano Lett.* **2012**, *12*, 2625.
- (110) Ahmed, A.; Gordon, R. Directivity Enhanced Raman Spectroscopy Using Nanoantennas. *Nano Lett.* **2011**, *11*, 1800.
- (111) Sands, H. S.; Demangeot, F.; Bonera, E.; Webster, S.; Bennett, R.; Hayward, I. P.; Marchi, F.; Smith, D. A.; Batchelder, D. N. Development of a Combined Confocal and Scanning Near-Field Raman Microscope for Deep UV Laser Excitation. *J. Raman Spectrosc.* **2002**, *33*, 730.
- (112) Aoki, H.; Hamamatsu, T.; Ito, S. Deep Ultraviolet Scanning Near-Field Optical Microscopy for the Structural Analysis of Organic and Biological Materials. *Appl. Phys. Lett.* **2004**, *84*, 356.
- (113) Taguchi, A.; Hayazawa, N.; Furusawa, K.; Ishitobi, H.; Kawata, S. Deep-UV Tip-Enhanced Raman Scattering. *J. Raman Spectrosc.* **2009**, *40*, 1324.
- (114) Park, K. D.; Kim, Y. H.; Park, J. H.; Park, J. S.; Lee, H. S.; Yim, S. Y.; Lee, Y. H.; Jeong, M. S. Ultraviolet Tip-Enhanced Nanoscale Raman Imaging. *J. Raman Spectrosc.* **2012**, *43*, 1931.
- (115) Veerman, J. A.; Garcia-Parajo, M. F.; Kuipers, L.; van Hulst, N. F. Single Molecule Mapping of the Optical Field Distribution of Probes for Near-Field Microscopy. *J. Microsc.* **1999**, *194*, 477.
- (116) Biagioni, P.; Polli, D.; Labardi, M.; Pucci, A.; Ruggeri, G.; Cerullo, G.; Finazzi, M.; Duo, L. Unexpected Polarization Behavior at the Aperture of Hollow-Pyramid Near-Field Probes. *Appl. Phys. Lett.* **2005**, *87*, 223112.
- (117) Minh, P. N.; Ono, T.; Tanaka, S.; Esashi, M. Spatial Distribution and Polarization Dependence of the Optical Near-Field in a Silicon Microfabricated Probe. *J. Microsc.* **2001**, *202*, 28.